American Mineralogist, Volume 93, pages 844–852, 2008

Fracture toughness, hardness, and elastic modulus of kyanite investigated by a depth-sensing indentation technique

Alexandre Mikowski,[1] Paulo Soares,[2] Fernando Wypych,[3] and Carlos M. Lepienski[1,*]

[1]Department of Physics, Universidade Federal do Paraná, Curitiba (PR) 81531-990, Brazil
[2]Department of Mechanical Engineering, Pontifícia Universidade Católica do Paraná, Curitiba (PR) 80215-901, Brazil
[3]Department of Chemistry, Universidade Federal do Paraná, Curitiba (PR) 81531-990, Brazil

Abstract

Macroscopically bladed kyanite crystals of blue and glassy luster were cleaved along two planes, and the mechanical properties were measured through depth-sensing indentation (DSI). The conventional method to determine fracture toughness (K_{IC}) from indentation is based on radial crack lengths measurements, which is difficult to estimate owing to the ease with which kyanite cleaves. An alternative method is proposed to determine the K_{IC} for the perfect cleavage plane (100) of kyanite based on the estimation of the crack nucleation threshold load from a discontinuity or "pop-in" in the DSI load-unload curve. The toughness value for kyanite in the plane of perfect cleavage (100) determined by the proposed method is K_{IC} =2.1 MPa·m$^{1/2}$. The hardness of 10.7 ± 1.6 GPa for the perfect cleavage plane is lower than the one measured in a plane (010), 18.0 ± 2.9 GPa. The measured elastic modulus for the perfect cleavage plane (100) and for the plane (010) are 297 ± 11 and 405 ± 31 GPa, respectively. These values are in agreement with the published mechanical properties of kyanite, obtained by other techniques. The mechanical behavior is discussed and correlated to fracture patterns during indentation for both crystallographic directions of this mineral.

Keywords: Kyanite, fracture toughness, hardness, elastic modulus, depth-sensing indentation, mechanical properties

Introduction

Kyanite, with an ideal composition of Al_2SiO_5, is the high-pressure polymorph of the aluminosilicate group, which includes two other minerals, andalusite, and sillimanite. The three polymorphs are very important in metamorphic and experimental petrology due to their abundance and relatively simple chemistry, providing an exemplary crystal-chemical system to study mineral transformations (Yang et al. 1997a). Kyanite is classified as an orthosilicate (isolated SiO_4 tetrahedra; i.e., no O atoms bridging to other Si tetrahedra) (Hatman and Sherriff 1991) with AlO_6 octahedra forming chains parallel to [001]. It occurs in metamorphic rocks and its color is variable, with blue, white, green, yellow, pink, gray, or black varieties known to occur, depending on the contaminant elements; Fe^{3+}, Cr^{3+}, and Ti^{4+} being the most important ones and generally substituting for octahedral Al. Kyanite is primarily used in refractory and ceramic products, including porcelain plumbing fixtures and dinnerware, as electrical insulators and abrasives, and as a gemstone, though this last application is limited by its anisotropic characteristic (Karaus and Moore 2003).

The structure of kyanite is triclinic with cell parameters: a = 7.1262 Å, b = 7.8520 Å, c = 5.5724 Å, α = 89.99°, β = 101.11°, and γ = 106.03° (Winter and Ghose 1979). Kyanite is strongly anisotropic, and its hardness varies depending on crystallographic direction, which is considered an identifying characteristic. The Mohs scale hardness of kyanite is ~4.5–5 when scratched in the direction of [001] (the octahedra chains) and ~6.5–7 when scratched perpendicular to this direction (Klein and Hurlbut 1999).

Aiming to study this anisotropic characteristic of the kyanite, Winchell (1945) measured the Knoop hardness (*HK*) using an applied load of 1 N. Due to the Knoop indenter geometry, the largest diagonal was oriented along the planes (001), (010), and (100) in combination with the directions [100], [010], and [001]. No cracks were observed for all the impressions. From the work of Winchell (1945), the averages Knoop hardness (*HK*) are 7.8 GPa for the cleavage plane (100) and 10.6 GPa for the other planes.

Recently, Whitney et al. (2007) carried out mechanical experiments using the Vickers indentation and depth-sensing indentation (Berkovich indenter) in some common metamorphic minerals with a single loading-unloading cycle with applied loads of 2 N and 100 mN, respectively. The three Al_2SiO_5 polymorphs (kyanite, andalusite, and sillimanite) were measured and presented Vickers hardness (*HV*) of 10–12 GPa and depth sensing indentation hardness (DSI) of 12–16 GPa, independent of the indented plane orientation.

The bulk modulus of kyanite was obtained through compress-

* E-mail: lepiensm@fisica.ufpr.br

ibility studies as 193 GPa (Yang et al. 1997a, 1997b) and 172 GPa (Comodi et al. 1997) through XRD studies. Winkler et al. (2001) obtained a bulk modulus for kyanite equal to 178 GPa using a density functional theory and 223 GPa using a core-shell model. Whitney et al. (2007) obtained the elastic modulus through depth-sensing indentation (DSI) and found an average value ranging from 186 to 253 GPa for the three planes. Although the mechanical properties of kyanite were extensively studied, the fracture processes generated during indentation were not thoroughly studied.

The conventional method to determine the fracture toughness from indentation is based on radial crack-length measurements, and for kyanite, the K_{IC} is difficult to estimate owing to the ease with which kyanite cleaves (Whitney et al. 2007). In this paper, a method to determine the fracture toughness for the perfect cleavage plane (100) of kyanite is proposed. This method is based on the estimation of the crack nucleation threshold load from a discontinuity or "pop-in" in the DSI load-unload curve. The Weibull statistic is used to determine the threshold load. This is done by establishing the mean value of the Weibull probability density functions (load at which there is a 50% fracture probability) as the minimum load to propagate the critical flaws, presented in the Lawn and Evans (1977) model. A closed expression is proposed to obtain the fracture toughness value. In addition, scratch hardness, indentation hardness, and elastic modulus are determined by depth-sensing indentation (DSI) in the perfect cleavage plane (100) and in the plane (010) for comparison.

Experimental methods

Blue kyanite specimens (10 × 10 × 3 mm³) from the state of Minas Gerais, Brazil were used to study the mechanical properties in two different crystalline directions. The purity of the sample and crystalline structure were confirmed through powder X-ray diffraction (XRD). The XRD patterns were recorded at room temperature in the 2θ range from 2 to 60 °2θ with a counting time of 1 °/min, operating at 40 kV and 40 mA, using Cu*K*α radiation (Shimadzu XRD-6000).

The samples were mechanically polished with successive grades of SiC papers (no. 600 to no. 1200) and alumina suspension (1 and ¼ μm) on both surfaces [planes (100) and (010)] before the indentation tests and roughness determination. Information on the topography of the surface and roughness was obtained by atomic force microscopy (Shimadzu SPM-9500J3). Four different zones were swept in each sample to perform a statistical analysis of the surface roughness. The images collected in the contact and dynamic modes were analyzed with the SPM-9500 software (Shimadzu).

The mechanical properties (indentation hardness, elastic modulus, and scratch hardness) were obtained using a Nanoindenter XP (MTS Instruments) (Oliver and Pharr 1992, 2004; Van Landingham 2003; Lepienski and Foerster 2004; Li et al. 1998; Sundararajan and Roy 2001). A set of 30 indentations (5 × 6) were made using a Berkovich tip (three sided pyramid), with applied loads from 0.8 to 400 mN corresponding to 12 complete loading-unloading cycles. Three 1000 μm long scratches were made using a Berkovich indenter with an indenter velocity of 10 μm/s and constant load of 400 mN. The scratch tests were performed in the [001] direction in the (100) plane, and in the [100] direction in the (010) plane.

The images of the indentation matrix, residual plastic impressions, fracture process, and scratch tests were collected on a scanning electron microscopy (Jeol JSM-6360 LV) using secondary and back-scattered electron signals at the Physics Department, CME-UFPR.

Analysis methodology

Roughness characterization

The average roughness, R_a, defined by (Johnson 1985) was determined using the following expression:

$$R_a = \frac{1}{L}\int_0^L |z|\,dx \tag{1}$$

where $z(x)$ is the surface height above the datum and L is the sampling length and root-mean-square or standard deviation R_{ms} of the surface height from the center-line defined by (Johnson 1985):

$$R_{ms}^2 = \frac{1}{L}\int_0^L z^2 dx\,. \tag{2}$$

The relationship between R_{ms} and R_a for a regular sinusoidal profile is

$$R_{ms} = \frac{\pi}{2\sqrt{2}} R_a$$

and for a Gaussian random profile is

$$R_{ms} = \left(\frac{\pi}{2}\right)^{1/2} R_a\,.$$

Scratch test

The scratch hardness is defined as the vertical normal load per unit load-bearing or contact and it is expressed by (Li et al. 1998; Sundararajan and Roy 2001):

$$H_S = \varepsilon \frac{P_N}{w^2} \tag{3}$$

where, P_N is the applied constant load, w is the groove width (measured using a microscope), and ε is a numeric constant, equal to 4 for a pyramidal tip.

Depth-sensing indentation

The hardness (H) is defined as the mean pressure that a material can support under a load, and is determined by (Oliver and Pharr 1992, 2004):

$$H = \frac{P_{max}}{A(h_c)} \tag{4}$$

where P_{max} is the maximum applied load, and $A(h_c)$ is the projected contact area function that corrects the Berkovich tip rounding effect. The elastic modulus of the material is determined by (Hertz 1896; Brotzen 1994):

$$E = \frac{1-\nu^2}{\left(\frac{1}{E_r} - \frac{1-\nu_i^2}{E_i}\right)} \tag{5}$$

where, E_r is the reduced elastic modulus, E_i and ν_i are the indenter elastic modulus and Poisson ratio, and E and ν are the elastic modulus and Poisson ratio of the material, respectively. For diamond, E_i = 1141 GPa and ν_i = 0.07 (Oliver and Pharr 1992, 2004). Based on the relationships developed by Sneddon (1965), an expression for the reduced elastic modulus, E_r (Oliver and Pharr 1992, 2004) was derived:

$$E_r = \frac{\sqrt{\pi}}{2\beta}\frac{S}{\sqrt{A(h_c)}} \tag{6}$$

where $S = (dP/dh)$ is the stiffness obtained experimentally from the upper part of the unloading curve, and β is a constant dependent on the indenter geometry, being equal to 1.034 for a triangular symmetry (Oliver and Pharr 1992, 2004; Brotzen 1994).

Weibull statistics

Considering the occurrence of discontinuities and "pop-in" during depth-sensing indentation curves, the cumulative probability function P_f in the Weibull statistics corresponding to the probability of occurrence of pop-in is given by (Weibull 1951; Mikowski et al. 2006):

$$P_f = 1 - \exp\left[-\left(\frac{P - P_u}{P_0}\right)^m\right] \quad (7)$$

where m is the Weibull modulus, P is the applied load, P_0 is a normalizing parameter, and P_u is the load below which no fracture events (discontinuities and or pop-in) are assumed to be nucleated. The Weibull parameter m is related to the dispersion of the strength: the lower the value, the more variable the strength is. For ceramics, m is usually 5–20 (Fischer-Cripps 2000). The mean and variance of data are calculated respectively by

$$\mu_{P_f} = P_0 \Gamma\left(\frac{1}{m} + 1\right) \quad (8)$$

and

$$\sigma^2_{P_f} = P_0^2 \left\{\Gamma\left(\frac{2}{m} + 1\right) - \left[\Gamma\left(\frac{1}{m} + 1\right)^2\right]\right\} \quad (9)$$

where $\Gamma(x) = (x - 1)$ is a gamma function of a real number $x > 1$.

The estimator of the cumulative probability function P_f defined by (Bergman 1984; Sullivan and Lauzon 1986) is

$$P_f = \frac{n - 0.5}{N} \quad (10)$$

where n is the n^{th} result in the set of N total number indentation tests employed. The works of Bergman (1984) and Sullivan and Lauzon (1986) evaluated different estimators by varying the number of samples. Their conclusion was that the estimator defined by Equation 10 gives the lowest variation of the mean value of m, and it is the most appropriate estimator when $N \geq 20$. This conclusion was also reached by Monte Carlo numerical simulations using different estimators (Bergman 1984; Sullivan and Lauzon 1986). Therefore, this estimator was used to calculate the experimental cumulative probability of failure. By plotting the data in a convenient log-log plot, it is easy to estimate the constants defined in Equation 7, which determine the Weibull distribution.

Results and discussion

Roughness characterization

AFM images of the sample surface on both the planes [plane (100) and (010)] are shown in Figure 1. It can be observed that both samples present uniformly rough surfaces after polishing, although the (010) plane has a rougher surface (Fig. 1b).

The values of average roughness R_a (Eq. 1) and root-mean-square R_{ms} (Eq. 2) were obtained from the analysis of four images of each surface. To know the surface profiles, R_{ms} was plotted as a function of R_a. Based on the angular coefficients of these plots, it is possible to know if the surfaces present regular sinusoidal or Gaussian random profiles. The angular coefficient is 1.34 ± 0.10 for the perfect cleavage plane (100) and 1.25 ± 0.06 for the plane (010). When compared to the Gaussian random profile (Johnson 1985), these values for perfect cleavage plane (100) and plane (010) present errors of 0.5 and 7.5%, respectively.

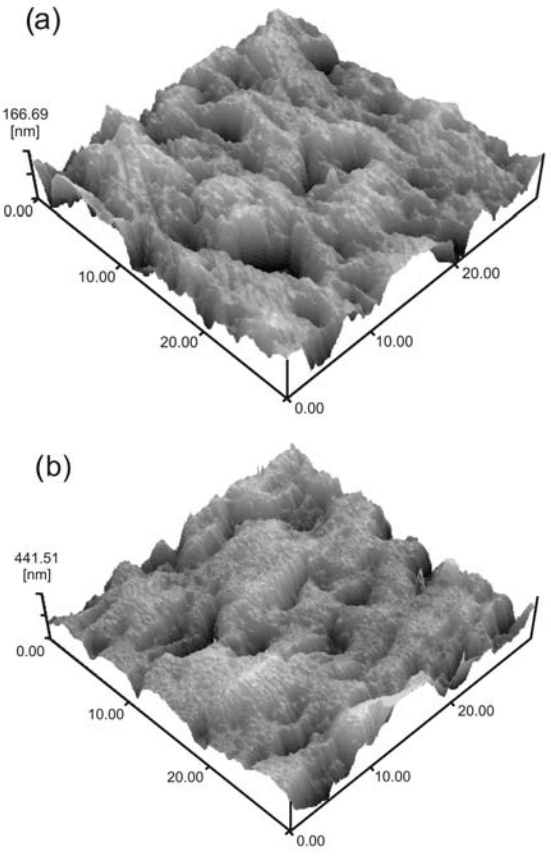

Figure 1. AFM images of the (**a**) plane of perfect cleavage (100), and (**b**) plane (010).

The average of the R_a is 33 ± 9 nm for the perfect cleavage plane (100) and 58 ± 13 nm for the plane (010). The average value of R_{ms} is 45 ± 13 nm for the perfect cleavage plane (100) and 75 ± 16 nm for the plane (010). The roughness determination is important since the mechanical properties assessed by depth-sensing indentation are affected by roughness (Mencík and Swain 1995).

Characterization by scratch test

Figure 2 shows SEM micrographs of scratch tracks on the plane of perfect cleavage (100) in the [001] direction (Fig. 2a) and the plane (010) in the [100] direction (Fig. 2b). All scratches were made with a Berkovich indenter and a constant applied load of 400 mN. Depending on the direction of the sample, a different behavior of the scratch hardness was observed. The micrograph of the cleavage plane (100) (Fig. 2a) shows a wider scratch. As this is the preferential cleavage plane, a larger track is formed, producing chipping or "delamination." The groove width was measured using an image analyzer software (UTHSCSA ImageTool program 2002) and is equal to 21.8 ± 2.3 μm for the cleavage plane (100) and 9.5 ± 0.8 μm for the plane (010). The scratch hardnesses calculated from Equation 3

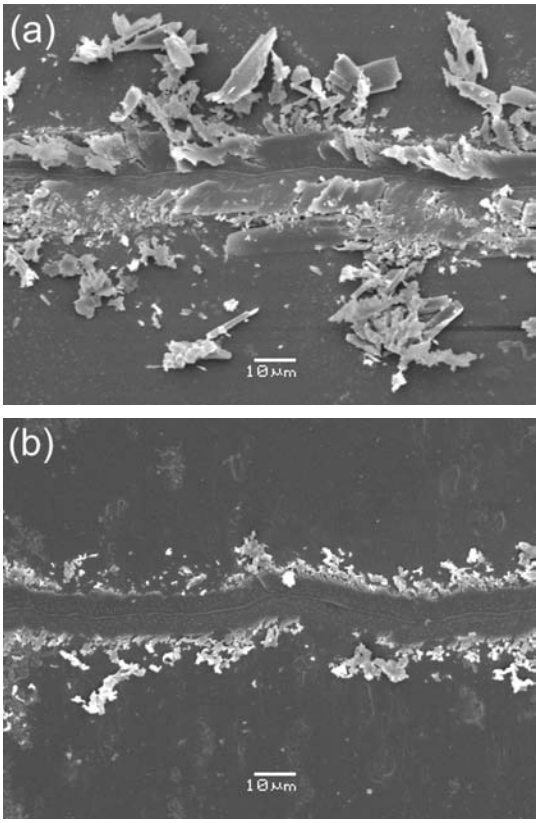

FIGURE 2. SEM micrographs showing scratch tracks on (**a**) in the [001] direction in the plane of perfect cleavage (100), and (**b**) in the [100] in the plane (010). The scratches were made using a Berkovich indenter with a constant applied load of 400 mN.

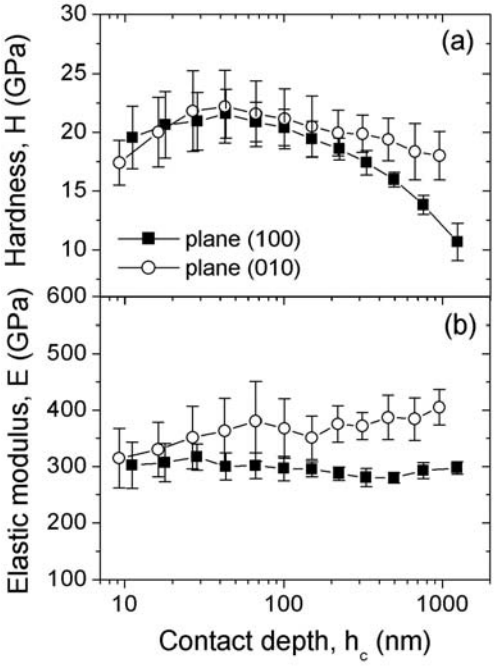

FIGURE 3. Hardness (**a**), and elastic modulus (**b**) as a function of displacement into surface of the plane of perfect cleavage (100) and the plane (010).

(Sundararajan and Roy 2001) are 3.35 ± 0.74 GPa and 14.35 ± 0.02 GPa, respectively.

According to the Mohs hardness scale (Klein and Hurlbut 1999), kyanite is ~4.5–5 when scratched along [001] in the cleavage plane (100) and ~6.5–7 when scratched perpendicular to [001] on (100) and (010). The results obtained from the scratch test are in agreement with the Mohs scale. However, as cited by West (1986), the Mohs scale is empirical and the numbers do not represent any regular mathematical ratio. In this context, the depth-sensing indentation is an appropriate technique to study the scratch resistance of minerals (Hangen 2001; Broz et al. 2006) and ceramic materials (Li et al. 1998; Houérou et al. 2003).

The resistance study of Na_2O-CaO-SiO_2 carried out by Houérou et al. (2003) shows three different regimes that appear during a typical scratch experiment: (1) micro-ductile regime; (2) micro-cracking regime; and (3) micro-abrasive regime. Figure 2 shows the micro-cracking and micro-abrasive regimes, these effects being more evident on the plane of perfect cleavage (100) (Fig. 2a). The micro-cracking regime is characterized by the formation of lateral cracks intersecting the surface and radial cracks. The micro-abrasive regime produces considerable debris, sometimes with small lateral cracks along the track that produce chipping.

Hardness and elastic modulus

Figure 3 shows the hardness and elastic modulus values as a function of displacement into the plane surface of the perfect cleavage (100) and the plane (010), obtained from the Equations 3 and 4. The scattering on the average values of hardness (H) and elastic modulus (E) for the indentation in the plane (010) are higher than the ones measured for the plane of perfect cleavage (100). This occurs due to the higher roughness of the plane (010). Thus, when the indentation is made on valley regions, the values are higher, and when the indentation is made in the crest, the H and E are lower than when made in a flat surface (Gunda et al. 2005; Souza et al. 2006). The surface roughness also affects the values of hardness at low penetration, in the order of the roughness measured by AFM. Even the best polished specimens have surface undulations with a height varying from several nanometers to several tens of nanometers (Mencík and Swain 1995). The effect of surface roughness on the indentation was studied by Bobji and Biswas (1999), who suggested that when the contact depth h_c is higher or equal to four times the value of the root-mean-square roughness R_{ms} ($h_c \geq 4\ R_{ms}$), the hardness values are reliable. Replacing the values of R_{ms} in this relation, the values of contact depth equal to 180 nm for the plane of perfect cleavage (100) and 300 nm for the plane (010) are found. For higher values of h_c, the magnitude of the scatter is quantified by a statistical non-dimensional parameter or variation coefficient (VC) and can be determined by the relation $VC = 100\% \times (\sigma/\mu)$, where σ is the standard deviation, and μ is the mean value of the hardness or elastic modulus for a given penetration depth

(Bobji et al. 1999). The *VC* values found for hardness and elastic modulus were lower than 15% for the plane of perfect cleavage (100) and 11.4% for the plane (010), which indicates that the values are statistically homogeneous.

Hardness variation of both planes (Fig. 3a) show similar behavior with displacement into surface up to about 500 nm, considering the error bar. Increasing the applied load, the hardness of the plane of perfect cleavage (100) tends to decrease due to the fractures generated during the indentation process. The hardness in the plane (010) is 18 ± 2 GPa, higher than the one in the plane of perfect cleavage (100), which is equal to 10.7 ± 1.6 GPa, for an applied load of 400 mN. The relation between the plane of perfect cleavage (100) and the plane (010) is about 1.6 for depth-sensing indentation tests. This relation is not observed for scratch hardness tests where the hardness in the plane (010) is four times the hardness in the plane of perfect cleavage (100). Results in the literature (Winchell 1945; Whitney et al. 2007) showed hardness values that are different according to the measurement technique used, which is commonly attributed to (1) indenter geometries (Knoop, Vickers, or Berkovich); (2) applied loads; (3) time at the maximum load; and (4) number of indentations. However, in this case, major effects are related to fracture events.

The values of elastic modulus (Fig. 3b) for indentations on the plane of perfect cleavage (100) have a value of 297 ± 11 GPa for an applied load of 400 mN. For the plane (010), the elastic modulus is 405 ± 31 GPa for the same applied load, which is ~1.4× the value for the plane of perfect cleavage (100). Whitney et al. (2007) determined the elastic modulus using depth-sensing indentation and found values ranging from 186 to 253 GPa for the three measured planes, for an applied load of 100 mN. Although few data of elastic modulus values are found in the literature, the bulk modulus was determined by several authors varying from 172 to 223 GPa. For isotropic materials, the elastic modulus can be calculated from bulk modulus using the relation $E = [3(1 - 2\nu)]K$, where ν is the Poisson ratio (Fischer-Cripps 2000). Using the value of ν = 0.24 (Soerensen 1996) and the expression above, the elastic modulus of kyanite was estimated as 301 GPa (Yang et al. 1997a, 1997b), 268 GPa (Comodi et al. 1997), and 278 and 348 GPa (Winkler et al. 2001). The value of the elastic modulus obtained through depth-sensing indentation in this work, 297 and 405 GPa, varies for the two different orientated surfaces. The discrepancies can be explained by the fractures produced during the indentation process.

Indentation fracture in the perfect cleavage plane (100)

Figure 4 shows representative curves of load (*P*) vs. displacement into the surface (*h*) from indentations on the plane of perfect cleavage (100) and the plane (010). A significant change was observed in the behavior of the curves in the range of 450–650 nm of penetration depth. This is evidenced by the presence of small discontinuities in the *P* vs. *h* of the perfect cleavage (100) plane, which is related to fracture events (Li and Bhushan 1998; Malzbender et al. 2000).

Figure 5 shows the SEM micrographs of Berkovich indentations for an applied load of 400 mN. The impressions on the plane of perfect cleavage (100) (Fig. 5a), show cracking and chipping around the indentations, which is not observed for the plane

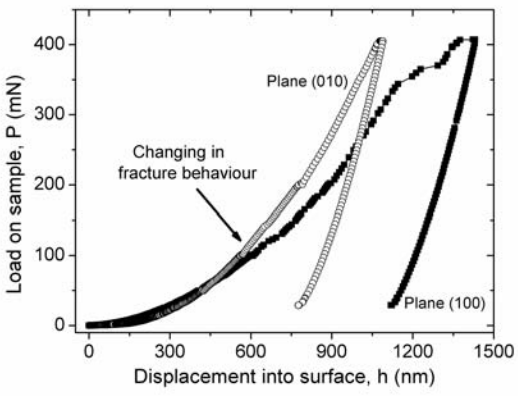

FIGURE 4. Typical *P* vs. *h* curves for the plane of perfect cleavage (100)—solid squares, and the plane (010)—open circles.

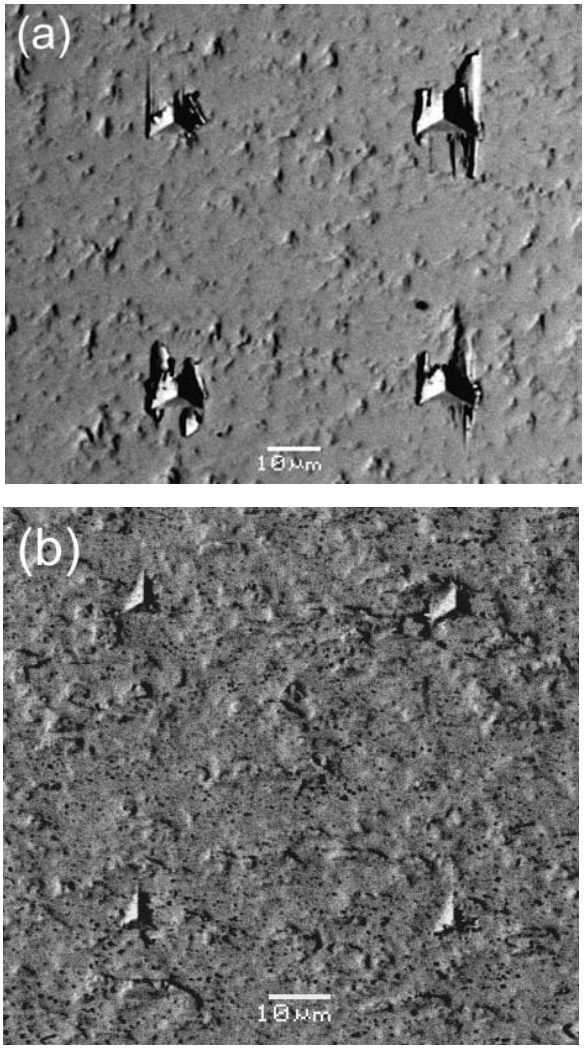

FIGURE 5. Back-scattered electron images showing Berkovich indentations on (**a**) plane of perfect cleavage (100), and (**b**) plane (010). Applied load of 400 mN. The bar denotes 10 µm.

(010) (Fig. 5b). It is also observed that the size of indentations on the plane (010) is smaller, which reflects on the higher values of hardness and elastic modulus. The fracture events observed on the *P* vs. *h* curve in Figure 4 are responsible for the difference between the values of hardness and elastic modulus on both planes. This feature was also observed by Winchell (1945) through Knoop microindentation, although an analysis of the fracture processes involved was not made.

Some fracture events appear in the *P* vs. *h* curves producing large abrupt discontinuities called "pop-in." A detailed investigation of each residual impression [perfect cleavage plane (100)] was made and is shown by representative SEM images in Figure 6. The occurrence of a fracture process including the formation of cracks (Fig. 6a) and chipping (Fig. 6b) is observed, which related to the discontinuities and "pop-ins" shown by arrows in the *P* vs. *h* curves (Figs. 6c and 6d). The smallest fracture events are the most difficult to see. That being so, these events were detected from the loading curve dP/dh^2 vs. h^2 (Malzbender and de With 2001). In Figures 6c and 6d, the discontinuities are fracture events related to the crack formation and the occurrence of "pop-ins," when there is an abrupt penetration of the indenter due to crack propagation and chipping. Figure 6a shows a situation where there is the occurrence of shallow lateral cracks (Cook and Pharr 1990) and Figure 6b shows the case where chipping occurs (Lepienski et al. 2006; Michel et al. 2006).

The "pop-ins" observed in the loading curve during DSI is a characteristic of layered materials. "Pop-ins" were observed in several materials such as intercalated hydrated cations in niobium disulfide (2H-NbS_2) (Lepienski et al. 2000), in the semiconductors InSe and GaSe (Mosca et al. 2002), layered crystals of lead iodide (Veiga and Lepienski 2002), and in graphite (Barsoum et al. 2004). "Pop-ins" were also observed for MgO crystals (Tromas et al. 2000), in semiconductors such as GaAs and Si (Leipner et al. 2001), $LiNbO_3$ (Bhagavat and Kao 2005), $Li_2B_4O_7$ (Stus et al. 2005), single-crystal Cr_3Si (Bei et al. 2005), GaN thin films (Navamathavan et al. 2006), and InGaN thin films (Jian et al. 2006). In non-layered materials, the authors suggest that the generation and increase of dislocations through Frank-Read sources are the plasticity mechanisms predominantly involved and related to the occurrence of "pop-ins" in the loading curve from depth-sensing indentation. In contrast, for layered materials, the "pop-ins" occur at higher loads, and they are predominantly related to layer fracture events.

Kyanite is not, strictly speaking, a layered material such as graphite; however, it presents a crystalline structure that has a perfect cleavage in the plane (100). As such, it presents a similar behavior to other phyllosilicates like micas. In addition, the values of load, where the "pop-ins" have been detected, are

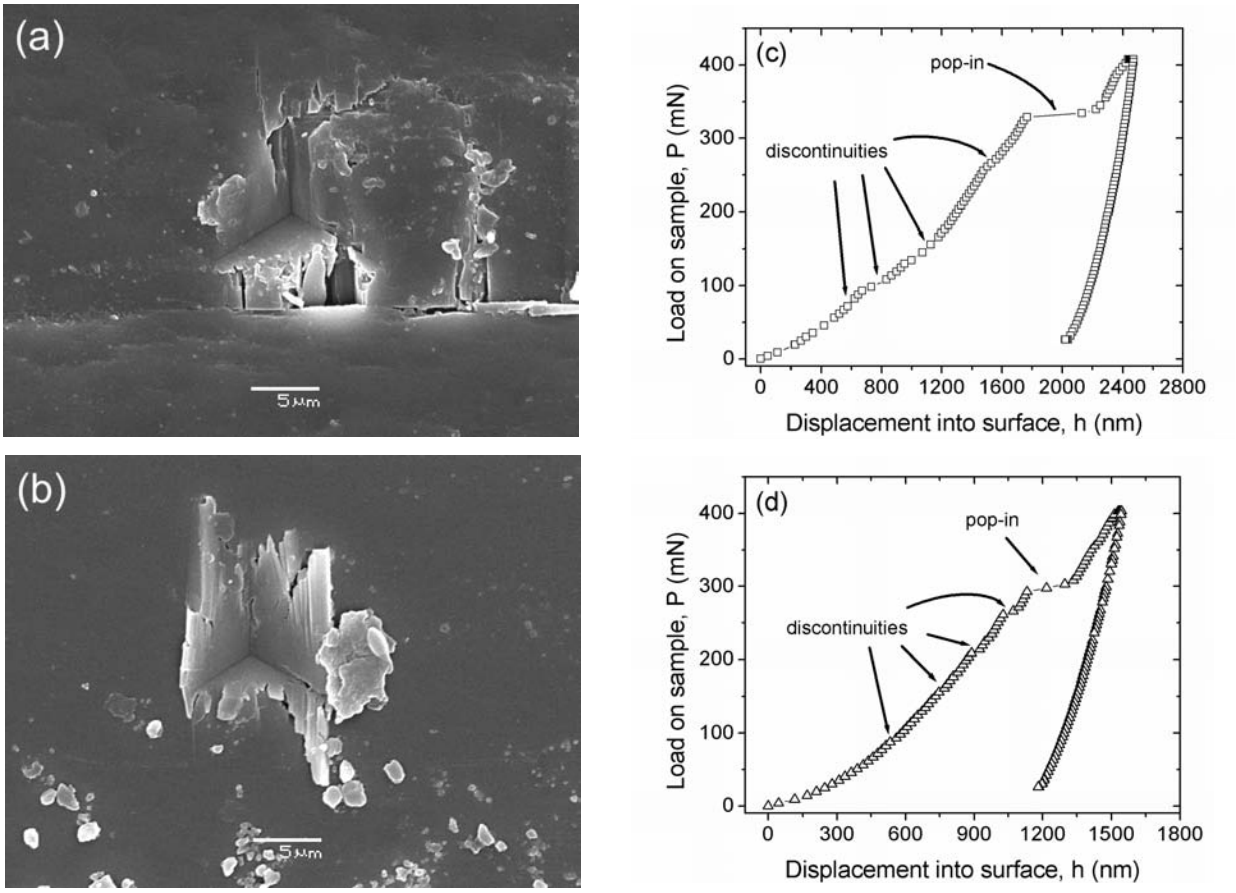

FIGURE 6. SEM micrographs (**a**) and (**b**) of residual impressions of Berkovich indenter with an applied load of 400 mN in the plane of perfect cleavage (100); (**c**) and (**d**) *P* vs. *h* curves. The bar denotes 5 μm.

much higher than the ones observed in the *P* vs. *h* curves for non-layered materials. Based on the fractographic analysis correlation with the *P* vs. *h* curves (Figs. 6c and 6d), the predominant deformation mechanisms related to "pop-ins" are attributed to (1) crack formation; (2) crack propagation; and (3) occurrence of chipping (Malzbender et al. 2000; Lepienski et al. 2006; Michel et al. 2006). The plasticity mechanisms involving dislocation mobility are present as we are dealing with a kyanite crystal, but the energy involved is much lower than the energy stored by the system to generate a "pop-in" (Figs. 6c and 6d) (Veiga and Lepienski 2002).

Fracture toughness in perfect cleavage plane (100)

Indentation tests on the plane (010) show higher values of hardness and elastic modulus because more bonds need to be broken along this direction. The crystal is more bulky compared to the behavior in the direction of the perfect cleavage plane, which contains more Si-O bonds (Biino and Groning 1998). During depth-sensing indentation tests with a Berkovich indenter on the surface of the (100) plane, the atomic bonds are submitted to triaxial stresses until their rupture. Discontinuities and pop-ins observed in the *P* vs. *h* curves (Figs. 6c and 6d) are then related to fracture events as suggested by previous studies (Li and Bhushan 1998; Malzbender et al. 2000; Michel et al. 2006; Lepienski et al. 2006).

Based on the atomistic model of kinetic crack growth in brittle solids (Lawn 1975), more energy is necessary to break the chemical bonds when the indentations are performed on the plane (010) compared to the cleavage plane (100). Fracture toughness of brittle materials is a measure of the energy released during fracture, and thus, of the strength of its chemical bonds. It is different from the hardness obtained by indentation or scratching, which is directly related to the type and density of the bonds in the analyzed plane, as can be observed in Figure 1. The fracture toughness (K_{IC}) is related to the elastic modulus (E) by the expression $\kappa_{IC}^2 = \frac{E}{1-\nu^2} G$, where ν is the Poisson ratio, and G is the energy release rate. The conventional method to determine fracture toughness from indentation, based on the length of radial cracks, is not adequate for kyanite because it is so easy to cleave "layered-like materials" like kyanite (Whitney et al. 2007).

In this work, a new method to determine fracture toughness based on the expression developed by Lawn and Evans (1977) is proposed. This method consists of the following steps: (1) estimation of the applied load (P) threshold for the crack nucleation through the best fit of the Weibull statistic function; (2) calculation of the Weibull modulus (m) and the scale parameter (P_0); (3) calculation of the load (P_C) at which there is a 50% fracture probability from the mean value (Eq. 8) of the Weibull probability density function; and (4) calculation of the fracture toughness using the following expression (Lawn and Evans 1977; Lawn and Marshall 1979):

$$P_C = 2.2\times10^4 \left(\frac{K_{IC}}{H}\right)^3 K_{IC}. \quad (11)$$

The minimum load to propagate the critical flaws presented by the Lawn and Evans (1977) model is considered as the critical load of 50% determined in step 3, or in other words, P_c = μ_{P_f} the mean value for Weibull statistics. Combining Equations 8 and 11, we have

$$K_{IC} = \left[\frac{P_0\Gamma\left(\frac{1}{m}+1\right)H^3}{2.2\times10^4}\right]^{1/4}. \quad (12)$$

This expression was used to estimate the fracture toughness of kyanite. In this model, it is considered that median cracks nucleate just below the indenter and their propagation occurs through the rupture of chemical bonds in the cleavage plane. When the applied load is increased, cracking and chipping occurs around the indentations (Figs. 5 and 6a–6b).

The applied load threshold for radial crack nucleation has been studied for soda-lime-silica glass using statistical models. Dal Maschio et al. (1984) used the Gauss distribution as the probability distribution function for the crack nucleation for Vickers indentations. Mikowski et al. (2006) used the 3 parameter Weibull statistics and estimated this threshold as 180 ± 5 mN, which was in agreement with the experimental results that pointed out a load threshold ranging from 100–200 mN. The locator parameter P_u (Eq. 7) is the level of the applied load P where there is no fracture on the material (Fischer-Cripps 2000) and thus, there is no discontinuity or "pop-in" in the P vs. h depth-sensing indentation curve. From 30 indentation tests made on the plane of perfect cleavage (100), discontinuities and "pop-ins" were not observed for applied loads lower than 57.8 mN. The locator parameter P_u was changed from 0 to 55 mN (with step of 5 mN) to check the best-fitting function representing the fracture probability. Figure 7 shows the plots of Equation 7, linearized for the data of applied load P where the first fracture event (discontinuity or "pop-in") was identified on the P vs. h curve. The Weibull modulus m, the scale parameter P_0, the standard deviation σ, and the linear fit correlation coefficient R were analyzed to check the best-fit function.

Figure 7 shows linear fit for $\ln\{\ln[1/(1-P_f)]\}$ against $\ln(P-P_u)$ for different values of P_u, which reveals that the experimental data can be described by the Weibull statistics. The two-parameter Weibull statistic was employed on Figure 7a, considering P_u equal to zero, whereas Figure 7b, a three-parameter Weibull statistic, was used assuming P_u equal to 50 mN. The Weibull module m and the scale parameter P_0 both underwent a decrease in value with the increase of the locator parameter P_u, but these two parameters are not enough to obtain the best fit. Considering P_u = 50 mN, the experimental data yield the best linear fit, the lower standard deviation σ, and the highest correlation coefficient R. The three-parameter Weibull statistic indicates good agreement with the experimental data obtained through depth-sensing indentation for P_u = 50 mN, where the probability of a fracture or the probability to find a discontinuity and/or a "pop-in" in the curve P vs. h is practically nil. Hence, the load threshold for the discontinuity or "pop-in" nucleation on the P vs. h curve occurs around P_u equal to 50 mN, according to the Weibull statistic

TABLE 1. Numerical values obtained from the Weibull statistics

m	P_0 (mN)	R	σ	P_u (mN)
2.78 ± 0.16	156 ± 94	0.96	0.37	0
1.51 ± 0.04	99 ± 23	0.99	0.17	50

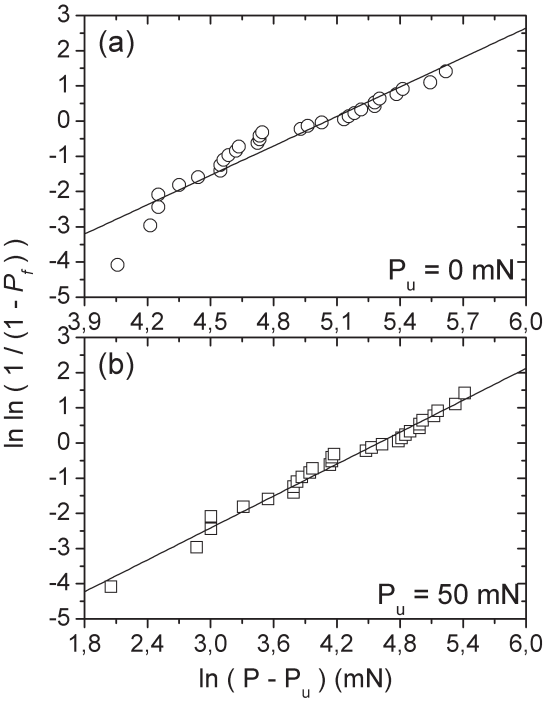

FIGURE 7. Weibull plots for the first fracture event in curve *P* vs. *h* as a function of the applied load.

model denoted by Equation 7. Experimentally, the minimum load threshold was 57.8 mN. Table 1 presents the main results of Weibull modulus (m), scale parameter (P_0), correlation coefficient (R), and standard deviation (σ) from the linear fit (Fig. 7) obtained varying the locator parameter (P_u).

Using the values of $P_0 = 99 \pm 23$ mN, $m = 1.51 \pm 0.04$, and $H = 17 \pm 1$ GPa (measured for $P = 50$ mN), in the equation of fracture toughness for the kyanite in the plane of perfect cleavage (100) is equal to $K_{IC} = 2.1 \pm 0.2$ MPa·m$^{1/2}$. This value is higher than the ones found for the kyanite polymorphs andalusite ($K_{IC} = 1.8 \pm 0.5$ MPa·m$^{1/2}$) and sillimanite ($K_{IC} = 1.6 \pm 1.5$ MPa·m$^{1/2}$) (Whitney et al. 2007).

ACKNOWLEDGMENTS

The authors thank CAPES and CNPq for the financial support, and the Electronic Microscopy Center (CME) at Universidade Federal do Paraná for lending the facilities.

REFERENCES CITED

Barsoum, M.W., Murugaiah, A., Kalidindi, S.R., Zhen, T., and Gogotsi, Y. (2004) Kink bands, nonlinear elasticity, and nanoindentations in graphite. Carbon, 42, 1435–1445.

Bei, H., George, E.P., Hay, J.L., and Pharr, G.M. (2005) Influence of indenter tip geometry on elastic deformation during nanoindentation. Physical Review Letters, 95, 1–4.

Bergman, B. (1984) On the estimation of the Weibull modulus. Journal of Materials Science Letters, 3, 689–692.

Bhagavat, S. and Kao, I. (2005) Nanoindentation of lithium niobate: Hardness anisotropy and pop-in phenomenon. Materials Science and Engineering A,393, 327–331.

Biino, G.G. and Groning, P. (1998) X-ray Photoelectron Spectroscopy (XPS) used as a structural and chemical surface probe on aluminosilicate minerals. European Journal of Mineralogy, 10, 432–437.

Bobji, M.S. and Biswas, S.K. (1999) Hardness of a surface uniformly spaced pyramidal asperities. Tribology Letters, 7, 51–56.

Bobji, M.S., Shivakumar, K., Alehossein, H., Venkateshwarlu, V., and Biswas, S.K. (1999) Influence of surface roughness on the scatter in hardness measurements—a numerical study. International Journal of Rock Mechanics and Mining Sciences, 36, 399–404.

Brotzen, F.R. (1994) Mechanical testing of thin films. International Materials Reviews, 39, 24–44.

Broz, M.E., Cook, R.F., and Whitney, D.L. (2006) Microhardness, toughness, and modulus of Mohs scale minerals. American Mineralogist, 91, 135–142.

Comodi, P., Zanazzi, P.F., Poli, S., and Schmidt, M.W. (1997) High-pressure behavior of kyanite: Compressibility and structure deformations. American Mineralogist, 82, 452–459.

Cook, R.F. and Pharr, G.M. (1990) Direct observation and analysis of indentation cracking in glasses and ceramics. Journal of the American Ceramic Society, 73, 787–817.

Dal Maschio, R., Maddalena, A., and Calliari, I. (1984) Radial crack initiation in glass by Vickers indentation. Materials Chemistry and Physics, 11, 443–451.

Fischer-Cripps, A.C. (2000) Introduction Contact Mechanics, 1st edition, p. 1–30. Springer-Verlag, New York.

Gunda, R., Biswas, S.K., Bhowmick, S., and Jayaram, V. (2005) Mechanical properties of rough TiN coating deposited on steel by cathodic arc evaporation technique. Journal of the American Ceramic Society, 88, 1831–1837.

Hangen, U.D. (2001) A comparision of nano-hardness and scratch-resistance on Mohs minerals. Zeitschrift Fur Metallkunde, 92, 1074–1077.

Hatman, J.S. and Sherriff, B.L. (1991) ^{29}Si MAS NMR of the aluminosilicate mineral kyanite: Residual dipolar coupling to ^{27}Al and nonexponential spin-lattice relaxation. Journal of Physical Chemistry, 95, 7575–7579.

Hertz, H. (1896) Miscellaneous Papers (translated by Jones, D.E. and Schott, G.A.), p. 178–180. Macmillan and Co., Ltd. London.

Houérou, V.L., Sangleboeuf, J.C., Dériano, S., Rouxel, T., and Duisit, G. (2003) Surface damage of soda-lime glasses: Indentation scratch behavior. Journal of Non-Crystalline Solids, 316, 54–63.

Jian, S.R., Fang, T.H., and Chuu, D.S. (2006) Nanomechanical characterizations of InGaN thin films. Applied Surface Science, 252, 3033–3042.

Johnson, K.L. (1985) Contact Mechanics, 1st edition, p. 406–411. Cambridge University Press, U.K.

Karaus, M. and Moore, R. (2003) Structure, properties, and behavior of kyanite: Use in refractory monolithics. Refractories Applications and News, 8, 11–36.

Klein, C. and Hurlbut Jr., C.S. (1999) Manual of Mineralogy, 21st edition, p. 682. John Wiley and Sons, New York.

Lawn, B.R. (1975) An atomistic model of kinetic crack growth in brittle solids. Journal of Materials Science, 10, 469–480.

Lawn, B.R. and Evans, A.G. (1977) A model for crack initiation in elastic/plastic indentation fields. Journal of Materials Science, 12, 2195–2199.

Lawn, B.R. and Marshall, D.B. (1979) Hardness, toughness, and brittleness: An indentation analysis. Journal of the American Ceramic Society, 62, 347–350.

Leipner, H.S., Lorenz, D., Zeckzer, A., Lei, H., and Grau, P. (2001) Nanoindentation pop-in effect in semiconductors. Physica B, 308–310, 446–449.

Lepienski, C.M. and Foerster, C.E. (2004) Nanomechanical properties by nanoindentation. In H.S. Nalwa, Ed., Encyclopedia of nanoscience and nanotechnology, p. 1–20. American Scientific Publishers, Stevenson Ranch, California.

Lepienski, C.M., Meruvia, M.S., Veiga, W., and Wypych, F. (2000) Mechanical properties of niobium disulfide and its hydrated sodium cation intercalation compound. Journal of Materials Research, 15, 2069–2072.

Lepienski, C.M., Michel, M.D., Araújo, P.J.G., and Achete, C.A. (2006) Indentation fracture of a-C:H thin films from chemical vapour deposition. Philosophical Magazine A, 86, 5397–5406.

Li, K., Shapiro, Y., and Li, J.C.M. (1998) Scratch test of soda-lime glass. Acta Materialia, 46, 5569–5578.

Li, X. and Bhushan, B. (1998) Measurement of fracture toughness of ultra-thin amorphous carbon films. Thin Solid Films, 315, 214–221.

Malzbender, J. and de With, G. (2001) The use of the indentation loading curve to detect fracture of coatings. Surface and Coatings Technology, 137, 72–76.

Malzbender, J., de With, G., and den Toonder, J.M.J. (2000) Elastic modulus, indentation pressure, and fracture toughness of hybrid coatings on glass. Thin Solid Films, 366, 139–149.

Mencík, J. and Swain, M.V. (1995) Error associated with depth-sensing microindentation tests. Journal of Materials Research, 10, 1491–1501.

Michel, M.D., Muhlen, L.V., Achete, C.A., and Lepienski, C.M. (2006) Fracture toughness, hardness, and elastic modulus of hydrogenated amorphous carbon films deposited by chemical vapor deposition. Thin Solid Films, 496, 481–488.

Mikowski, A., Serbena, F.C., Foerster, C.E., and Lepienski, C.M. (2006) Statistical analysis of threshold load for radial crack nucleation by Vickers indentation in commercial soda-lime silica glass. Journal of Non-Crystalline Solids, 352, 3544–3549.

Mosca, D.W., Mattoso, N., Lepienski, C.M., Veiga, W., Mazaro, I., Etgens, V.H., and Eddrief, M. (2002) Mechanical properties of layered InSe and GaSe single crystals. Journal Applied Physics, 91, 140–144.

Navamathavan, R., Moon, Y.T., Kim, G.S., Lee, T.G., Hahn, J.H., and Park, S.J.

(2006) "Pop-in" phenomenon during nanoindentation in epitaxial GaN thin films on c-plane sapphire substrates. Materials Chemistry and Physics, 99, 410–413.

Oliver, W.C. and Pharr, G.M. (1992) An improved technique for determining hardness and elastic modulus using load and displacement sensing indentation experiments. Journal of Materials Research, 7, 1564–1583.

——— (2004) Measurement of hardness and elastic modulus by instrumented indentation: Advances in understanding and refinements to methodology. Journal of Materials Research, 19, 3–20.

Sneddon, I.N. (1965) The relation between load and penetration in the axisymmetric Boussinesq problem for a punch of arbitrary profile. International Journal of Engineering Science, 3, 47–57.

Soerensen, M. (1996) Seismic reflectivity of the lower crust investigating the role of anisotropy. M.Sc. thesis, Institute of General Geology, University of Copenhagen.

Souza, G.B., Foerster, C.E., Silva, S.L.R., and Lepienski, C.M. (2006) Nanomechanical properties of rough surfaces. Materials Research, 9, 159–163.

Stus, N.V., Dub, S.N., Stratiychuk, D.A., and Lisnyak, V.V. (2005) Pop-in effect at nanoindentation of lithium tetraborate (100) face. Journal of Alloys and Compounds, 403, 305–307.

Sullivan, J.D. and Lauzon, P.H. (1986) Experimental probability estimators for Weibull plots. Journal of Materials Science Letters, 5, 1245–1247.

Sundararajan, G. and Roy, M. (2001) Hardness testing. In K.H.J. Buschow, R.W. Cahn, M.C. Flemings, B. Ilschner, E.J. Kramer, S. Mahajan, and P. Veyssière, Eds., Encyclopedia of Materials: Science and Technology, p. 3728–3736. Elsevier Science Ltd., Oxford.

Tromas, C., Girard, J.C., and Woirgard, J. (2000) Study by atomic force microscopy of elementary deformation mechanisms involved in low load indentations in MgO crystals. Philosophical Magazine A, 80, 2325–2335.

UTHSCSA ImageTool V 3.0 (2002) Program developed at the University of Texas Health Science Center at San Antonio, Texas and available from the Internet by anonymous FTP from ftp://maxrad6.uthscsa.edu.

Van Landingham, M.R. (2003) Review of instrumented indentation. Journal of Research oh the National of Standards and Technology, 108, 249–265.

Veiga, W. and Lepienski, C.M. (2002) Nanomechanical properties of lead iodide (PbI_2) layered crystals. Materials Science and Engineering A, 335, 6–13.

Weibull, W. (1951) A statistical distribution function of wide applicability. Journal of Applied Mechanics—Transactions ASME, 18, 293–297.

Whitney, D.L., Broz, M., and Cook, R.F. (2007) Hardness, toughness, and modulus of some commom metamorphic minerals. American Mineralogist, 92, 281–288.

Winchell, H. (1945) The Knoop microhardness tester as a mineralogical tool. American Mineralogist, 30, 583–595.

Winkler, B., Hytha, M., Warren, C.M., Milman, V., Gale, J.D., and Schreuer, J. (2001) Calculation of the elastic constants of the Al_2SiO_5 polymorphs andalusite, sillimanite, and kyanite. Zeitschrift für Kristallographie, 216, 67–70.

Winter, J.K. and Ghose, S. (1979) Thermal expansion and high-temperature crystal chemistry of the Al_2SiO_5 polymorphs. American Mineralogist, 64, 573–586.

West, G. (1986) An observation on Mohs scale of hardness. Quarterly Journal of Engineering Geology, 19, 203–205.

Yang, H., Downs, R.T., Finger, L.W., Hazen, R.M., and Prewitt, C.T. (1997a) Compressibility and crystal structure of kyanite, Al_2SiO_5, at high pressure. American Mineralogist, 81, 467–474.

Yang, H., Hazen, R.M., Downs, R.T., Finger, L.W., and Prewitt, C.T. (1997b) Compressibility and crystal structure of sillimanite, Al_2SiO_5, at high pressure. Physics and Chemistry of Minerals, 25, 39–47.

MANUSCRIPT RECEIVED MAY 14, 2007
MANUSCRIPT ACCEPTED NOVEMBER 30, 2007
MANUSCRIPT HANDLED BY FLORIAN HEIDELBACH